Separation and Purification Technology 274 (2021) 118987

Contents lists available at ScienceDirect

Separation and Purification Technology

journal homepage: www.elsevier.com/locate/seppur

Mass transfer and kinetic characteristics for CO_2 absorption in microstructured reactors using an aqueous mixed amine

Mohsin Pasha [a], Guangxiao Li [a], Minjing Shang [a], Saier Liu [a], Yuanhai Su [a,b,*]

[a] School of Chemistry and Chemical Engineering, Frontiers Science Center for Transformative Molecules, Shanghai Jiao Tong University, Shanghai 200240, PR China
[b] Key Laboratory of Thin Film and Microfabrication (Ministry of Education), Shanghai Jiao Tong University, Shanghai 200240, PR China

ARTICLE INFO

Keywords:
CO_2 absorption
Mass transfer
High gas to liquid flow rate ratio
Microreactors
Multi-objective optimization

ABSTRACT

Microreactors are frequently used for the process intensification of CO_2 absorption, but most CO_2 absorption studies in microreactors are restricted to a low flow rate ratio of feed gas to absorbent because of insufficient CO_2 loading of conventional amines. Herein, we investigated mass transfer and kinetic characteristics of CO_2 absorption using an aqueous mixed amine absorbent composed of 25 wt.% N-methyldiethanolamine (MDEA) and 5 wt.% hexamethylenediamine (HMDA) at the gas to liquid flow rate ratio range from 88.9 to 666.7 in four microstructured reactors with metal foams as packing materials in the packed-bed section. The CO_2 loading of this amine absorbent reached 0.32 mol of CO_2 per mol of MDEA at the gas to liquid flow rate ratio of 400, which is significantly higher than the conventional amines. Regeneration efficiency of this mixed amine absorbent was remarkable in three successive regenerated cycles at the gas to liquid flow rate ratios of 181.8 and 222.2. The second-order rate constants of HMDA were higher than the conventional amines, reflecting its high ability to reduce energy barrier and accelerate the CO_2 absorption rate. The overall volumetric mass transfer coefficient and absorption efficiency were raised to 13.5 s^{-1} and 97% at the gas to liquid flow rate ratios of 153.8 and 88.9, which are obviously higher than those reported for other microreactors. Optimization of overall reaction rate constant and mass transfer coefficient was executed through multi-objective optimization using genetic algorithm and validated through experimentation. Finally, the comparison of the mass transfer characteristics among various microreactors indicated that the strategy of combining this remarkable mixed amine absorbent with microstructured reactors with metal foams packing has strong process intensification potential for CO_2 absorption at high gas to liquid flow rate ratios.

1. Introduction

Thriving concentration of carbon dioxide (CO_2) in atmosphere has become one of the serious concerns in current era. Gigatons of CO_2 are emitted into atmosphere every year [1,2], giving rise to serious environmental repercussions, such as global warming, rising sea level [3] and reduction in crop production [4]. Amine-based absorption is the most matured and cost-effective process to capture CO_2 from flue gases [5–7]. However, inadequate mass transfer is a lasting problem in conventional absorbers, stemming from low specific interfacial area and weak interfacial forces. Furthermore, energy penalty of a plant is increased by 25–40% with the use of the conventional amine absorbents [8,9].

Microreactors provide a systematic gateway to improve the mass transfer characteristics for the CO_2 absorption. They have fascinating features, such as extensively large specific surface area [10], excellent mixing performance [11–14], fast heat and mass transfer rates [15–17], high selectivity [18], inherently safe attributes [19–21], and precise control over process parameters [22]. High specific interfacial area and excellent transport abilities of microreactors are highly advantageous to overcome the mass transport resistance across the phases boundaries and accelerate the CO_2 absorption rate. Because of these fascinating characteristics, microreactors are widely used for process intensification of CO_2 absorption. However, the fabrication cost of microreactors with comparable operational throughput is significantly higher than conventional reactors for CO_2 absorption such as sieve plate column, spray column, agitated bubble reactor, and so on.

Hydrodynamic and mass transfer characteristics for CO_2 absorption

* Corresponding author at: School of Chemistry and Chemical Engineering, Frontiers Science Center for Transformative Molecules, Shanghai Jiao Tong University, Shanghai 200240, PR China.
E-mail address: y.su@sjtu.edu.cn (Y. Su).

https://doi.org/10.1016/j.seppur.2021.118987
Received 4 January 2021; Received in revised form 14 May 2021; Accepted 15 May 2021
Available online 24 May 2021

have been frequently examined in microreactors. For instance, Ganapathy et al. [23] investigated overall mass transfer coefficient and interfacial area in slug and churn flow patterns by using three different microreactors with inner diameters of 0.254 mm, 0.508 mm and 0.762 mm, respectively. These parameters reached 400 s^{-1} and 15000 m^2/m^3, which were two to four orders and one to two orders of magnitude higher than those of the conventional absorbers. Yao et al. [24] executed outstanding process intensification of CO_2 absorption using deionized water and diethanolamine (DEA) absorbents in a numbered-up microreactor at elevated pressure. Pan et al. [25] examined the CO_2 absorption in activated methyldiethanolamine (A-MDEA), which was a blend of N-MDEA and piperazine (PZ), using high throughput microporous tube-in-tube microchannel reactor (MTMCR). The overall mass transfer coefficient and absorption efficiency were raised to 1.70 s^{-1} and 97% at the feed gas and absorbent throughputs of 100 L/h and 5.32 L/h, respectively. Recently, Sang et al. [26] analyzed hydrodynamic and mass transfer characteristics for CO_2 absorption in aqueous N-methyldiethanolamine (N-MDEA) by using micropacked bed reactor with open cell metal foams as packing materials. The metal foams have higher porosity and specific area than conventional packing materials [27], and tortuous flow paths inside the metal foams give rise to high mass transport [28]. Because of these fascinating characteristics of metal foams, high mass transfer coefficients were obtained at the expense of low pressure drop in this micropacked bed reactor.

Assessment of overall mass transfer coefficient and absorption efficiency was restricted to a low flow ratio of feed gas and absorbent in most studies. This restriction was stemmed from the insufficient CO_2 uptake ability of conventional amines, such as monoethanolamine (MEA) and diethanolamine (DEA), used in these studies [23,29–31]. Furthermore, these amines are highly corrosive in aqueous media and exhibit low cyclic capacity that is determined from the difference of CO_2 concentration in rich and lean solutions. Mixed or blended amine, such as activated MDEA (A-MDEA) and a blend of N-MDEA and DEA, was used in some studies [32–35], but no appreciable improvement was observed in mass transfer performance at high gas to liquid flow rate ratios.

Recently, Mondal et al. [36] examined the reaction kinetics of CO_2 absorption using an aqueous mixed amine, i.e., the mixture of N-MDEA and hexamethylenediamine (HMDA), in a reaction calorimeter. Interestingly, the CO_2 absorption rate was enormously improved by the small addition of HMDA. For instance, the overall rate constant of the aqueous mixed amine absorbent (25 wt.% MDEA + 5 wt.% HMDA) was 41 times higher than that of the aqueous 30 wt.% MDEA [36], and the absorption rate of this mixed amine was 14% higher than that of another aqueous mixed amine (25 wt.% MDEA + 5 wt.% PZ) [37].

In this work, we applied the aqueous mixed amine absorbent (25 wt.% MDEA + 5 wt.% HMDA) to investigate the mass transfer and kinetic characteristics of CO_2 absorption in four microstructured reactors (MSRs) with metal foams as packing materials. These investigations were carried out at high gas to liquid flow rate ratio, ranging from 88.9 to 666.7. Various geometrical and operating parameters, such as MSR size, temperature, concentration, and gas to liquid flow rate ratio were studied to better understand the mass transfer and kinetic mechanisms. We investigated regeneration efficiency of this amine absorbent in three successive regenerated cycles and optimized the overall kinetic rate constant and mass transfer coefficient by using multi-objective optimization based on genetic algorithm. Finally, comparison of the mass transfer characteristics among various microreactors was performed to analyze the potential improvement made by this remarkable amine absorbent at high gas to liquid flow rate ratios.

2. Experimental section

2.1. Materials

N-methyldiethanolamine (MDEA, purity 99%) was purchased from Macklin (Shanghai Macklin, Co., Limited, China). 1,6 Hexanediamine (HMDA, purity 99%) was provided by Damas-beta (Shanghai Titan Scientific Co. Limited, China). The feed gas mixture consisted of 10% CO_2 and 90% N_2 (v/v) was supplied by Air Liquid Co., Limited (Shanghai, China). The gas composition was confirmed through gas chromatography (GC, GC-6600, Shanghai Fanwei Instrument Equipment CO., Limited, China) prior to performing experiments. Deionized water was used to prepare the aqueous mixed amine absorbent with the composition of 25 wt% MDEA and 5 wt% HMDA. Both amines were directly used for experiments without further treatment.

Open cell metal foams, fabricated with Ni and Cr, were purchased from Taili Metal Work (Suzhou, China). Two different sizes of metal foams, with the average diameters of 2.5 mm (MF-1) and 4.0 mm (MF-2), were used in the microstructured reactors. Three-dimensional visualization of metal foams was executed through X-ray microscope Zeiss Xradia 520 Versa to analyze its structural properties, such as pore per inch (PPI), pore diameter, porosity and surface area to volume ratio (m^2/m^3). Structural view of these metal foams can be viewed from Fig. 1, and two images of these metal foams obtained from the X-ray microscope are presented in Fig. S1 (Supporting Information).

Image processing software Dragonfly Pro was used to evaluate the structural parameters for MF-1. Detail procedure for measuring these parameters is provided in the Supporting Information. Pore size dataset was generated by measuring various pore sizes, as shown by Fig. S2 (Supporting Information). Mean pore size of metal foams was determined from the distribution of a pore size dataset by using normal, logistic and lognormal methods, as shown in Fig. 2. The lowest standard deviation in pore size measurement was found to be 0.14 by using lognormal distribution. Therefore, the mean pore size was reported by considering the lognormal distribution of a pore size dataset. Structural parameters of MF-1 are listed

in Table 1. These structural properties of metal foams are fundamentally required to develop a correlation of overall volumetric mass transfer coefficient (k_La) in terms of dimensionless Reynold (Re) and Weber (We) numbers as indicated by several studies [26,38]. However, the overall volumetric mass transfer coefficient was directly correlated to the gas to liquid flow rate ratio and the temperature in this work, and this correlation was developed for the microstructured reactor (MSR-2) with packing MF-1. Therefore, the characterization of metal foams was only restricted to MF-1.

2.2. Experimental setup

The schematic diagram of the experimental setup is represented by Fig. 3. Microstructured reactor was primarily composed of two sections,

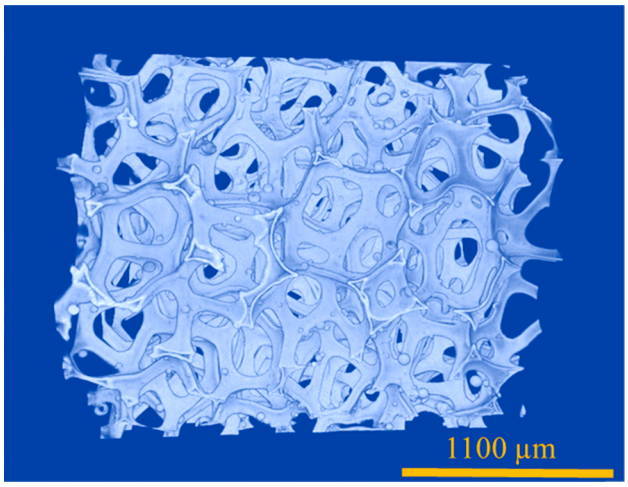

Fig. 1. Structural view of metal foams (MF-1).

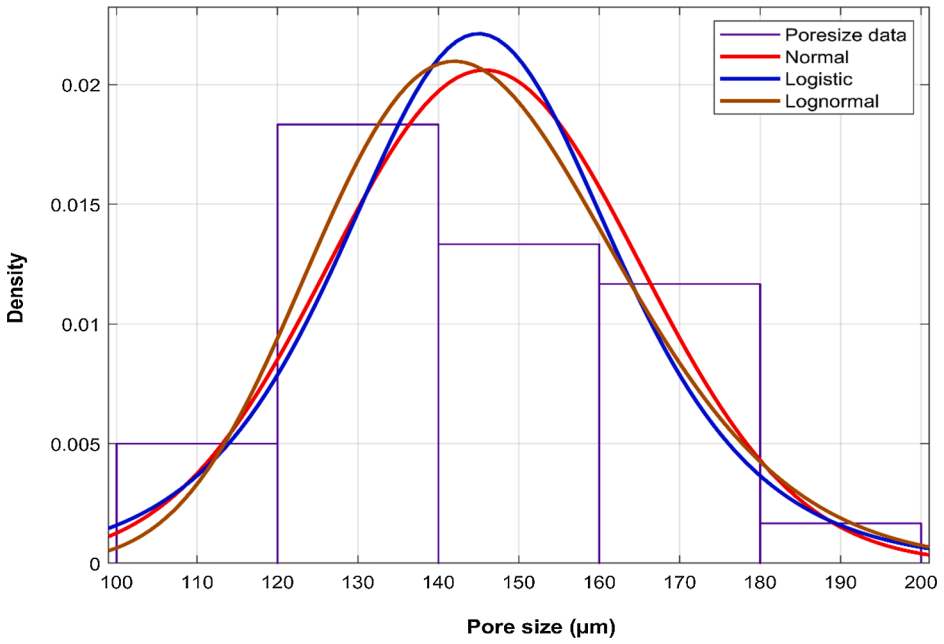

Fig. 2. Various distribution plots for the pore size determination of metal foams.

Table 1
Structural parameters of MF-1 metal foams.

Parameters	Measured Values
Porosity	0.72
Mean pore size (μm)	145.7
Pore per inch (PPI)	200
Surface area to volume ratio (m^2/m^3)	1555.6

i.e., packed-bed and empty, which were connected through a connector to restrict the movement of metal foams. Perfluoroalkoxy (PFA) tubes (Valco Instruments, CO., Limited, United states) were used to establish these sections, and metal foams were inserted in the packed-bed section tube as suggested in several studies [26,39]. Four microstructured reactors with different sizes, including MSR-1, MSR-2, MSR-3 and MSR-4 were used to analyze the mass transfer characteristics of CO_2 absorption. Packed-bed section tubes of MSR-1 and MSR-2 had an identical inner diameter of 2.5 mm and metal foams with the same size (2.5 mm) were used inside these tubes. However, empty section tubes of MSR-1 and MSR-2 had the inner diameters of 2.5 mm and 2.0 mm, respectively.

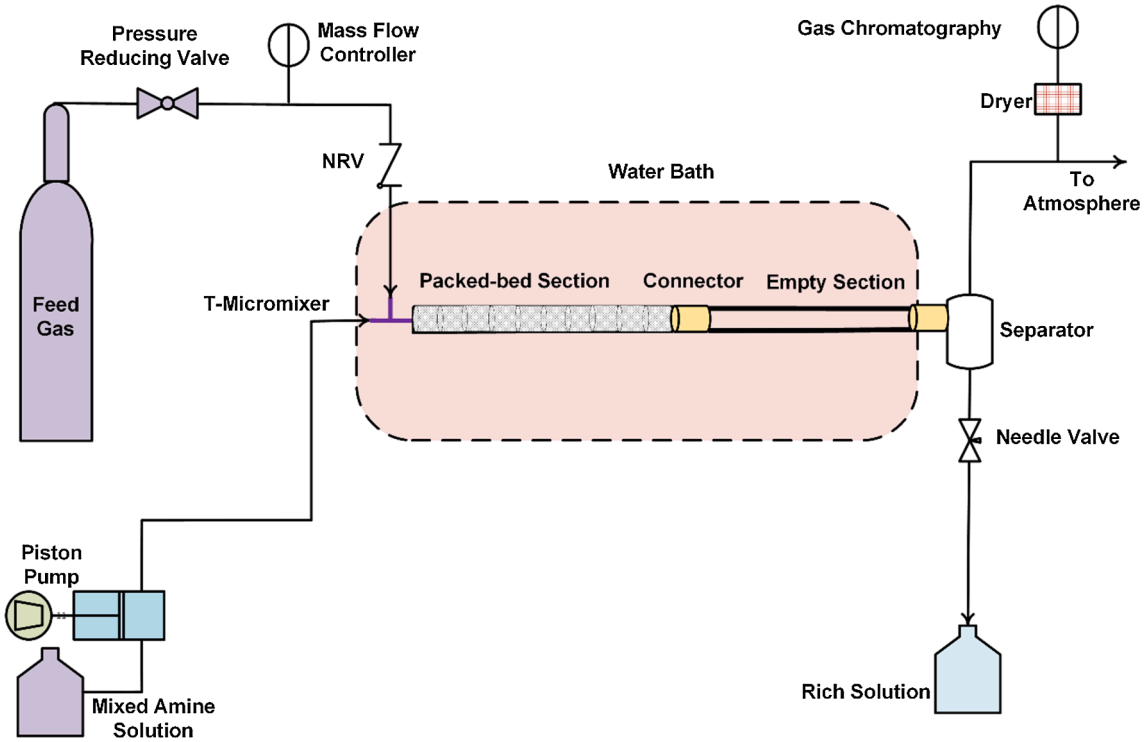

Fig. 3. Schematic diagram of experimental setup.

Similarly, MSR-3 and MSR-4 had the same size of the packed-bed section tubes but different sizes of the empty section tubes, as mentioned in Table 2.

The feed gas composed of 10% CO_2 and 90% N_2 (v/v) was supplied through a cylinder. A mass flow controller with a flow range of 0–500 ml/min and a non-return valve were installed on the gas line. A mixed amine absorbent with a concentration of 25 wt.% MDEA and 5 wt.% HMDA was introduced through a piston pump. The operating ranges of the feed gas and absorbent flow rates were 40–100 ml/min and 0.15–0.45 ml/min, respectively. The feed gas flow rate was measured under atmospheric conditions ($P = 1$ atm and $T = 25$ °C). The whole microstructured reactor system was submerged into a water bath to maintain the operating temperature within the range of 30–60 °C. A homemade phase separator, fabricated through 3D printer (Formlab form 2), was applied to ensure the fast separation of the gas and liquid phases, which was beneficial for the reduction of end effects.

2.3. Measurement of overall volumetric mass transfer coefficient

Overall volumetric mass transfer coefficient (k_La) was determined from CO_2 absorption flux (N_{CO2}) and log-mean concentration difference of CO_2 (ΔC_{CO2}). N_{CO2} was calculated from Eq. (1):

$$N_{CO_2} = \frac{\Delta n_{CO_2}}{aV} = \frac{n_{CO_2 in} - n_{CO_2 out}}{aV} \tag{1}$$

where the parameters $n_{co2\ in}$, $n_{co2\ out}$, a and V were the molar flow rate of CO_2 at the inlet and outlet of MSR, specific interfacial area and volume of MSR, respectively. ΔC_{CO2} was evaluated from the interfacial concentration of CO_2 ($C^*_{CO_2}$) at the inlet and outlet of MSR [23], and it was determined by applying Henry Law, with the use of partial pressure (P_{CO2}) and Henry constant (H_{CO2}). Since the liquid volumetric flow rate was quite low in this investigation and the porosity of metal foams (MF-1) was significantly larger than conventional packing materials, the pressure drop and its impact on the measurement of k_La were neglected.

$$k_L = \frac{N_{CO_2}}{\Delta C_{CO_2}} \tag{2}$$

$$k_La = \frac{\Delta n_{CO_2}}{V \Delta C_{CO_2}} \tag{3}$$

$$\Delta C_{CO_2} = \frac{C^*_{CO_2 in} - C^*_{CO_2 out}}{\left(ln \frac{C^*_{CO_2 in}}{C^*_{CO_2 out}} \right)} = \frac{1}{H_{CO_2}} \left(\frac{P_{CO_2 in} - P_{CO_2 out}}{ln \frac{P_{CO_2 in}}{P_{CO_2 out}}} \right) \tag{4}$$

The N_2O analogy was used to determine the H_{CO2} for amine. Henry constants of CO_2 and N_2O for water were calculated by using Eqs. (5) and (6) [4], and H_{N2O} for this amine (25 wt.% MDEA + 5 wt.% HMDA) was evaluated from the physical solubility data of N_2O taken from the literature [36]. Then, H_{CO2} for the amine was calculated from Eq. (7). Likewise, the diffusivity of CO_2 (D_{CO2}) in this amine was assessed through the N_2O analogy. Diffusivities of CO_2 and N_2O in water were calculated from Eqs. (8) and (9) [4], and the revised Stokes-Einstein equation (Eq. (10)) was used to determine D_{N2O} in amine by using viscosities of amine and water, and D_{CO2} in amine was evaluated from Eq. (11). The value of γ for aqueous MDEA was taken as 0.8 [4]. The estimated H_{CO2} and D_{CO2} values for this amine absorbent at the temperature range of 30–60 °C are listed in Table 3.

$$H_{CO_2,water} = 2.8249 \times 10^6 exp\left(\frac{-2044}{T}\right) \tag{5}$$

$$H_{N_2O,water} = 8.5470 \times 10^6 exp\left(\frac{-2284}{T}\right) \tag{6}$$

$$H_{CO_2,amine} = H_{N_2O,amine} \times \frac{H_{CO_2,water}}{H_{N_2O,water}} \tag{7}$$

$$D_{CO_2,water} = 2.35 \times 10^{-6} exp\left(\frac{-2119}{T}\right) \tag{8}$$

$$D_{N_2O,water} = 5.07 \times 10^{-6} exp\left(\frac{-2371}{T}\right) \tag{9}$$

$$D_{N_2O,amine} \mu^{\gamma}_{amine} = D_{N_2O,water} \mu^{\gamma}_{water} \tag{10}$$

$$D_{CO_2,amine} = D_{N2O,amine} \times \frac{D_{CO_2,water}}{D_{N_2O,water}} \tag{11}$$

The absorption efficiency (η) and CO_2 loading (α) were determined by using Eqs. (12) and (13). All experiments were repeated at least three times under each operating condition, and average values of these parameters (i.e., k_La, η and α) were finally reported.

$$\eta = \frac{n_{CO_2 in} - n_{CO_2 out}}{n_{CO_2 in}} \times 100 \tag{12}$$

$$\alpha = \frac{mol\ of\ CO_2}{mol\ of\ MDEA} \tag{13}$$

2.4. Measurement of overall kinetic rate constant

Overall kinetic rate constant (k_{ov}) was determined by the subsequent reactions of CO_2 with MDEA, HMDA and H_2O. MDEA reacts with CO_2 through the base-catalyzed mechanism (Scheme 1). Presence of water is essential in this reaction as MDEA cannot directly react with CO_2 because of the absence of proton, and thus hydration of CO_2 leads to the bicarbonate ion (HCO_3^-) formation.

In Scheme 1, $k_{2,MDEA}$ and k_{-2} indicate the forward and reverse rate constants. Reaction between CO_2 and HMDA proceeds through the zwitterion mechanism (Scheme 2). The nucleophilic amine addition in the electrophilic carbon atom of CO_2 results in the zwitterion formation, which upon deprotonation leads to the carbamate formation. Potential bases for this deprotonation reaction are MDEA, HMDA, H_2O and OH^- [36,40].

$k_{2,HMDA}$ and k_{-1} are the forward are reverse rate constants of the zwitterion formation, while k_B represents the rate constant of the deprotonation reaction in Scheme 2, which includes k_{MDEA}, k_{HMDA}, k_{H2O} and k_{OH}^-. Here, B indicates the bases involved in this reaction, including MDEA, HMDA, H_2O and OH^-. Addition of water in CO_2 leads to the carbonic acid and bicarbonate formation, as presented by the following

Table 2
Details of microstructured reactors (MSRs).

Microstructured Reactor	Packed-bed section		Empty section	
	Length (cm)	ID (mm)	Length (cm)	ID (mm)
MSR-1	5.0	2.5	5.0	2.5
MSR-2	5.0	2.5	5.0	2.0
MSR-3	5.0	4.0	5.0	3.0
MSR-4	5.0	4.0	5.0	2.0

Table 3
Properties of the applied mixed amine composed of 25 wt.% MDEA and 5 wt.% HMDA.

Temperature (°C)	Density* (g/ml)	Viscosity* (cP)	Diffusivity × 10^9 (m^2/s)	Henry Constant (kPa. L/mol)
30	1.0150	2.89	0.723	3750
40	1.0101	2.10	1.021	4244
50	1.0043	1.59	1.399	4745
60	0.9976	1.24	1.872	5208

*These values are taken from the literature [36].

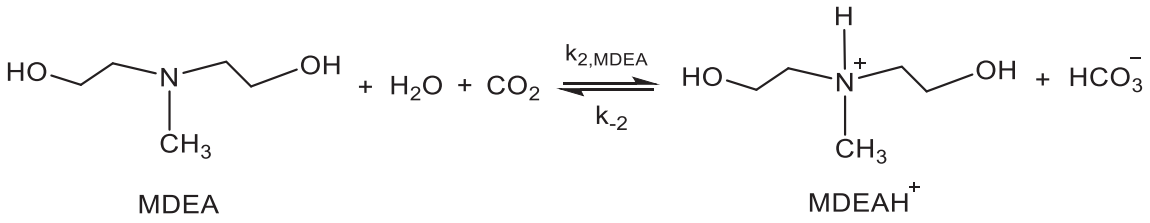

Scheme 1.

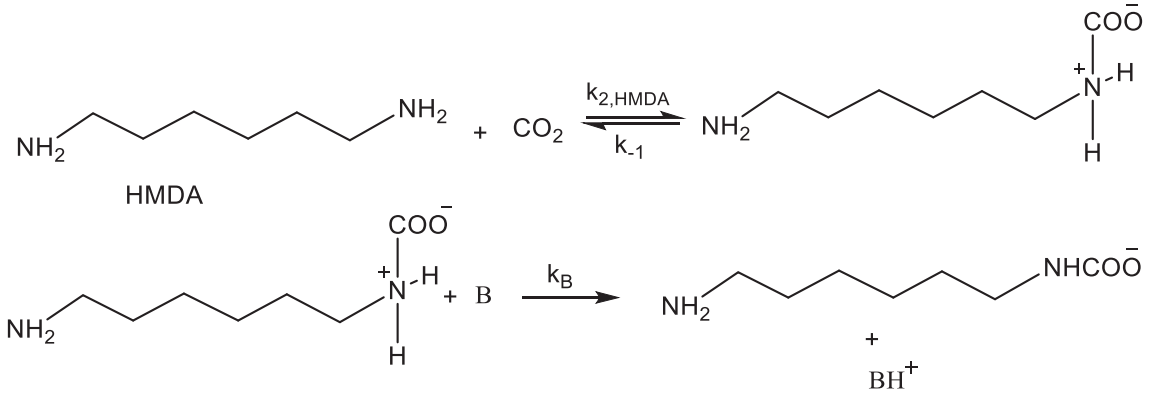

Scheme 2.

reactions (Scheme 3).

Rate constant of the carbonic acid formation reaction is very small (k_{H2O} = 0.026 s^{-1} at 298 K), and contribution of this reaction in the overall rate constant can be neglected [36]. Similarly, bicarbonate formation reaction does not show any significant influence on the overall reaction rate constant because of the limited concentration of hydroxyl ion (OH^{-1}) [41]. Consequently, the overall reaction rate depends on the CO_2 reactions with MDEA and HMDA (Schemes 1 and 2), as presented by following kinetic equations:

$$r_{ov} = r_{CO_2-MDEA} + r_{CO_2-HMDA} \tag{14}$$

$$r_{ov} = k_{2,MDEA} C_{MDEA} C_{CO_2} + \frac{C_{HMDA} C_{CO_2}}{\frac{1}{k_{2,HMDA}} + \frac{1}{\frac{k_{2,HMDA}k_{H_2O}}{k_{-1}} C_{H_2O} + \frac{k_{2,HMDA}k_{MDEA}}{k_{-1}} C_{MDEA} + \frac{k_{2,HMDA}k_{HMDA}}{k_{-1}} C_{HMDA}}} \tag{15}$$

$$r_{ov} = \left(k_{2,MDEA} C_{MDEA} + \frac{C_{HMDA}}{\frac{1}{k_{2,HMDA}} + \frac{1}{\frac{k_{2,HMDA}k_{H_2O}}{k_{-1}} C_{H_2O} + \frac{k_{2,HMDA}k_{MDEA}}{k_{-1}} C_{MDEA} + \frac{k_{2,HMDA}k_{HMDA}}{k_{-1}} C_{HMDA}}} \right) C_{CO_2} \tag{16}$$

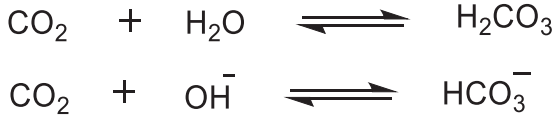

Scheme 3.

$$k_{ov} = \left(k_{2,MDEA} C_{MDEA} + \frac{C_{HMDA}}{\frac{1}{k_{2,HMDA}} + \frac{1}{\frac{k_{2,HMDA}k_{H_2O}}{k_{-1}} C_{H_2O} + \frac{k_{2,HMDA}k_{MDEA}}{k_{-1}} C_{MDEA} + \frac{k_{2,HMDA}k_{HMDA}}{k_{-1}} C_{HMDA}}} \right) \tag{17}$$

$$r_{ov} = k_{ov} C_{CO_2} \tag{18}$$

The overall rate constant was determined by assuming the pseudo-first-order (PFO) reaction condition. Under this condition, the dimensionless Hatta number (*Ha*) is considered to be equal to the enhancement factor (*E*), provided that the value of *Ha* is greater than 3 [35,42]. The enhancement factor was determined by the ratio of the mass transfer coefficients obtained from the chemical and physical absorptions [23]. The physical mass transfer coefficient ($k_{Lphysical}$) was estimated from the Higbie's penetration model, as indicated by Eq. (19). The chemical mass transfer coefficient (k_L) was evaluated from Eq. (3). The specific interfacial area could be assumed to equal to the specific surface area of MSR at high gas to liquid flow rate ratios because of small thickness of liquid film compared to the size of MSR [43,44]. Under each operating condition, six values of k_{ov} were evaluated, and the average of these values was finally reported. Its details are provided in the Supporting Information (Table S1 and Fig. S3).

$$k_{Lphysical} = 2\sqrt{\frac{D_{CO_2}}{\pi\tau}} \tag{19}$$

$$\tau = \frac{V}{Q_G + Q_L} \tag{20}$$

$$E = \frac{k_L}{k_{Lphysical}} \tag{21}$$

$$E = \sqrt{1 + Ha^2} \tag{22}$$

$$Ha = \frac{\sqrt{k_{ov} D_{CO_2}}}{k_{Lphysical}} \tag{23}$$

3. Results and discussion

3.1. Mass transfer characteristics analysis

Firstly, mass transfer characteristics were examined by evaluating overall volumetric mass transfer coefficient and absorption efficiency (η) in all four MSRs for a wide range of the gas to liquid flow rate ratio (88.9–666.7). Fig. 4 indicates the influence of the gas to liquid flow rates on k_La in these MSRs. As expected, there was a sharp rise in k_La by increasing the liquid flow rate. The liquid film around the gas core was rapidly saturated due to the low amine concentration, and the enhancement of liquid flow rate prevented the rapid saturation of this liquid film and led to the intensification of k_La in these MSRs [35]. Interestingly, it exhibited an inverse relationship with the gas flow rate that was against of its behavior observed in previous studies [23,29,45]. It could be explained from the two-phase flow pattern. In former studies, k_La was investigated at the low flow rate ratio of feed gas to absorbent, where the two-phase flow pattern was confined to slug or Taylor flow. The enhancement of the gas flow rate triggered significant rise in the specific interfacial area in the Taylor flow pattern that led to the improvement of the overall volumetric mass transfer coefficient in these studies. However, the two-phase flow pattern was changed to the annular flow regime due to the high flow rate ratio of the feed gas to absorbent in these MSRs. This flow regime was composed of wavy-annular and annular flow patterns [46] and contained a continuous gas phase in the form of annular core surrounded by a thin liquid film. Small fraction of gas contacted with liquid at this high gas holdup, and further increase in the gas flow rate possibly reduced the specific interfacial area due to the insufficient interfacial contact of gas and liquid resulting in the reduction of k_La in these MSRs [47].

The mass transfer performance of these MSRs can be ranked in the following order, i.e., MSR-2 > MSR-1 > MSR-4 > MSR-3. Smaller sizes of metal foams and capillaries in MSR-2 delivered higher superficial velocities of gas and liquid phases in both packed-bed and empty sections that resulted in higher k_La compared to the other MSRs. Moreover, tortuous flow paths inside these small metal foams proved to be highly beneficial for accelerating the mass transfer rate. It is worth noting that the value of k_La obtained in MSR-2 at the gas to liquid flow ratio of 88.8 was 36%, 72% and 62% higher than those of MSR-1, MSR-3 and MSR-4, respectively. Investigation of k_La was confined to the limited flow rate ratio of feed gas to absorbent in previous studies because of insufficient CO_2 uptake ability of conventional amines. For instance, Ganapathy et al. [30] used aqueous DEA absorbent in numbered-up microreactor and reported maximum CO_2 loading and k_La were 0.12 mol of CO_2/mol of amine and 17 s^{-1} at the gas to liquid flow rate ratios of 28.5 and 14.5, respectively. Conversely, CO_2 loading and k_La by using this aqueous amine absorbent (25% MDEA + 5% HMDA) in MSR-2 were raised to 0.32 mol of CO_2 / mol of MDEA and 13.5 s^{-1} at the gas to liquid flow rate ratios of 400 and 153.8, respectively. These statistics clearly indicated that the remarkable CO_2 loading of this mixed amine absorbent led to the better mass transfer performance of MSR-2 compared to the numbered-up microreactor used by Ganapathy et al. [30]. Detailed comparison between MSR-2 and the other microreactors regarding these key performance indicators is presented in Section 3.7.

Fig. 5 indicates the influence of the gas to liquid flow rate ratio on the absorption efficiency in these MSRs. MSR-2 showed higher absorption efficiency than the other MSRs because of its superior mass transfer performance. It should be noted that the enhancement of absorption efficiency became more pronounced at high gas to liquid flow rate ratios in MSR-2, e.g., the absorption efficiency in MSR-2 at the gas to liquid flow rate ratio of 400 was 12.1%, 13.8% and 7.5% higher than that of MSR-1, MSR-3 and MSR-4, respectively. However, the absorption efficiency was reduced by increasing the gas to liquid flow rate ratio in all MSRs. Reduction of the residence time by increasing the gas to liquid

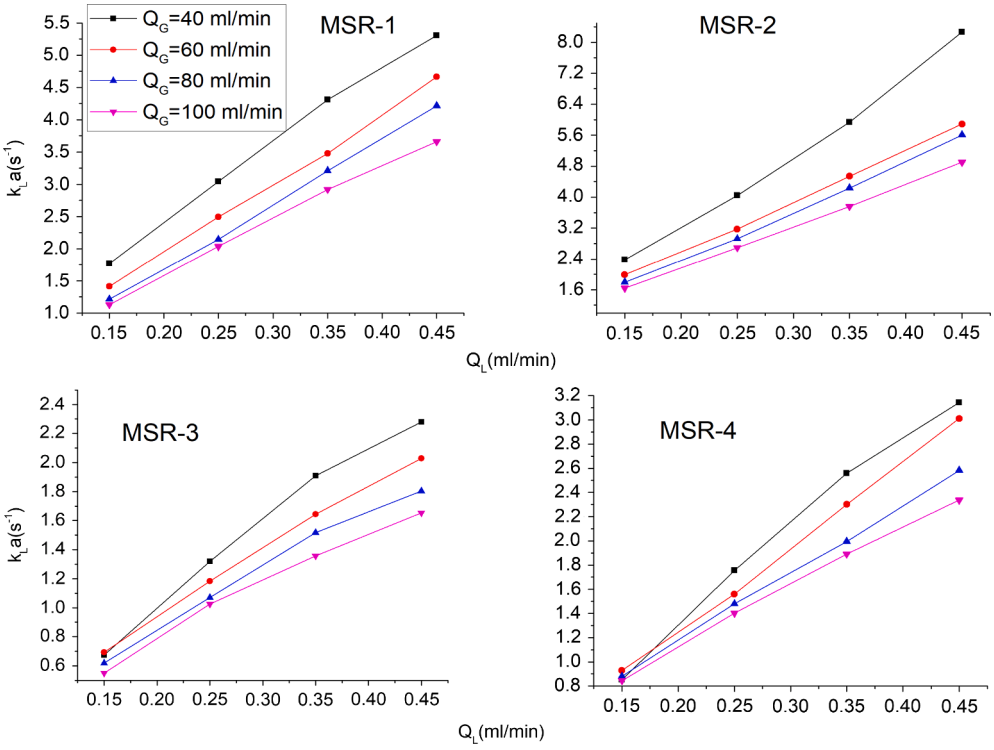

Fig. 4. Influence of the gas and liquid flow rate on overall mass transfer coefficient measured at 30 °C and 1 atm using amine absorbent (25 wt.% MDEA + 5 wt.% HMDA) in four MSRs.

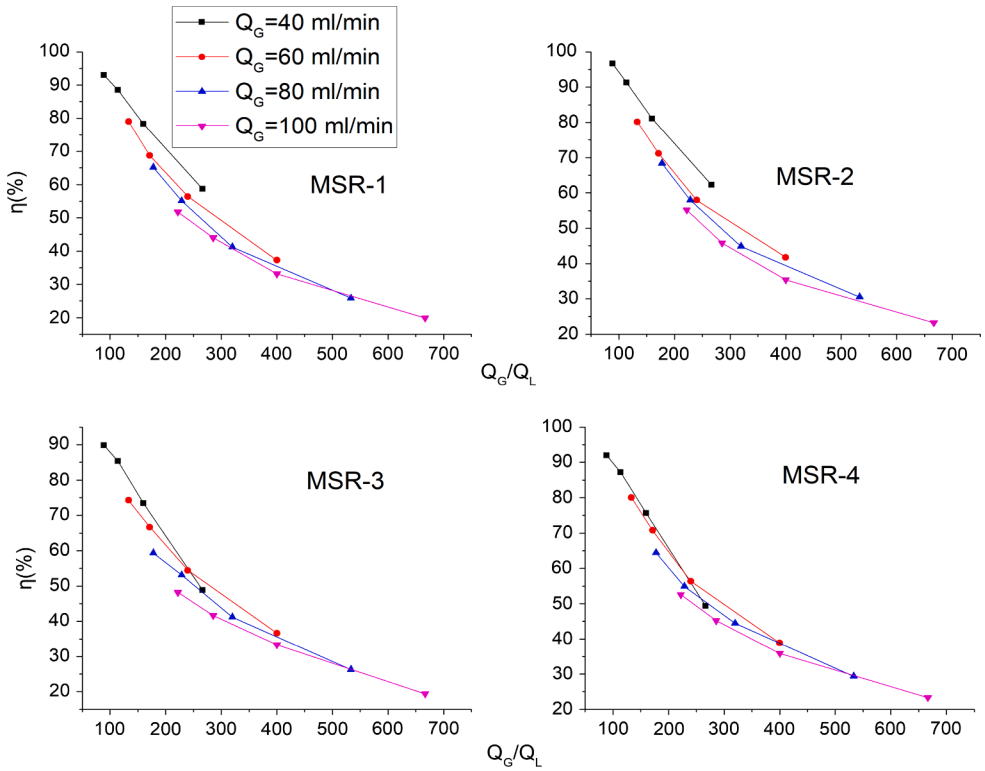

Fig. 5. Influence of the gas to liquid flow rate ratio on absorption efficiency evaluated at 30 °C and 1 atm using amine absorbent (25 wt% MDEA + 5 wt% HMDA) in four MSRs.

flow rate ratio led to decrease in axial and radial mass transport [31] that resulted in the alleviation of the absorption efficiency in these MSRs [35]. Similar trend of absorption efficiency with the gas to liquid flow rate ratio was found in several studies [23,29].

In previous studies, the enhanced absorption efficiency was achieved at the expense of high absorbent flow rates that indicated the insufficient CO_2 uptake ability of these absorbents. For instance, Aghel et al. [32] reported 100% absorption efficiency by using MEA and DEA absorbents at the gas to liquid flow rate ratio of 25, and Ganapathy et al. [29] stated the absorption efficiency was close to 100% by using DEA absorbent at the feed gas to absorbent flow rate ratio of 5. High absorption efficiency was achieved at the low gas to liquid flow rate ratio in both studies. In contrast, the absorption efficiency was raised to 97% in MSR-2 at the gas to liquid flow rate ratio of 88.9 showing excellent CO_2 uptake ability of this aqueous amine absorbent compared to the conventional amines. Based on better mass transfer performance of MSR-2, parametric and kinetic studies were performed by using this MSR.

3.2. *Effect of temperature on mass transfer performance*

This section summarizes the influence of temperature on the overall mass transfer coefficient and absorption efficiency, which can be elucidated by several ways. Firstly, the temperature enhancement gives rise to high reaction rate that triggers fast absorption flux. Most importantly, viscosity of absorbent is significantly reduced by increasing temperature that greatly expedites the diffusion of CO_2 in the absorbent. Conversely, temperature rise shifts the equilibrium of CO_2 absorption to the reverse direction and promotes the CO_2 desorption [32]. Secondly, the solubility of CO_2 in amines considerably drops with rising the temperature. Therefore, the temperature increase has both positive and negative influences on the CO_2 absorption.

Fig. 6 shows the influence of temperature on the overall volumetric mass transfer coefficient and the absorption efficiency. Interestingly, both parameters were improved by rising the temperature from 30 to

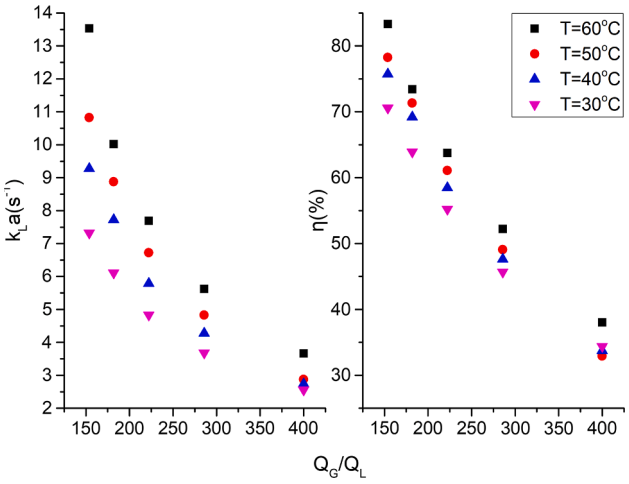

Fig. 6. Influence of temperature on overall mass transfer coefficient and absorption efficiency by using mixed amine absorbent (25 wt.% MDEA + 5 wt.% HMDA) at 1 atm in MSR-2.

60 °C. It should be noted that the viscosity of this mixed amine (25 wt.% MDEA + 5 wt.% HMDA) absorbent was reduced from 2.89 to 1.24 cP and the CO_2 diffusivity was increased from 0.723×10^{-9} to 1.872×10^{-9} m^2/s by rising the temperature that potentially led to the improvement in k_La and absorption efficiency. Furthermore, the enhancement of these parameters by rising the temperature was strongly influenced by the gas to liquid flow rate ratio. There was sharp improvement in the overall mass transfer coefficient and the absorption efficiency by increasing the temperature at the low gas to liquid flow rate ratios, but it shifted to gradual enhancement at higher gas to liquid flow rate ratios. For instance, k_La obtained at 60 °C was almost double of that at 30 °C at the gas to liquid flow rate ratio of 153.8, but this enhancement was reduced

to 1.4 times at the gas to liquid flow rate ratio of 400.

3.3. Effect of absorbent concentration on mass transfer performance

Absorbent concentration plays an important role in the mass transfer characteristics. Increase of absorbent concentration provides greater driving force and more reactive sites for the CO_2 absorption [32]. However, rise of the absorbent concentration enhances the absorbent viscosity to certain extent that impedes the mass transport. Typically, this effect is not so influential in aqueous amine and the rise of absorbent concentration normally leads to the enhancement in mass transfer. Since HMDA was a promotor in this mixed amine absorbent, its concentration was crucial in thriving the CO_2 absorption rate. Fig. 7 indicates the influence of the various concentrations of MDEA and HMDA on the CO_2 loading and absorption efficiency. It is worth noting that the CO_2 loading and absorption efficiency of aqueous mixed amine (29 wt.% MDEA + 1 wt.% HMDA) were eight and five times higher than those of aqueous MDEA (30 wt% MDEA), indicated that small addition of HMDA in aqueous MDEA showed great potential to improve the mass transfer performance of MSR-2. Further increase of the HMDA concentration (3–5 wt.%) triggered significant enhancement in these parameters, and the maximum CO_2 loading achieved by using 5 wt% HMDA was 0.32 mol of CO_2 /mol of MDEA at the gas to liquid flow rate ratio of 400, which was seventeen times higher than that of aqueous 30 wt.% MDEA and much higher than the conventional amines used for CO_2 absorption in previous studies [24,30].

Excellent CO_2 uptake ability of HMDA can be elucidated from its molecular configuration. It was claimed in some studies that the presence of electron withdrawing group (—OH) in conventional amines, such as MEA and DEA, reduced the electron density of the nitrogen atom of amine group (—NH_2) resulting in the lower basicity of these amines compared to HMDA [48,49]. We investigated this effect by executin g the computational studies on the HMDA, MEA and DEA molecular structures by using Gaussian 09 software package. The geometry and frequency optimization of these structures was performed by using the B3LYP density functional theory method with a basis set of 6-31+g(d), and CPCM was used as a solvation model. Fig. 8 shows the optimized structures of HMDA, MEA and DEA. It should be noted that the partial atomic charge on the nitrogen atom in DEA was 40% lower than that of the HMDA nitrogen atom due to presence of multiple —OH groups, but the nitrogen atom in MEA had slightly lower partial atomic charge compared to that of HMDA nitrogen atom due to single —OH group. Higher partial atomic charge on the nitrogen atoms in HMDA made it superior than conventional amines. Thus, these findings well agreed with the theoretical perspectives about these molecular structures as

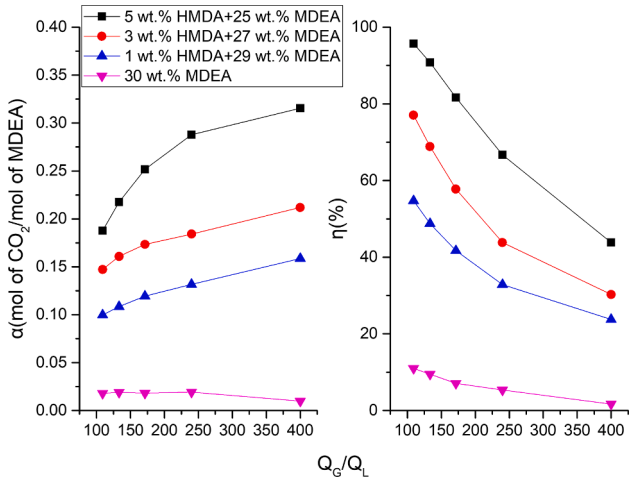

Fig. 7. Influence of absorbent concentration on CO_2 loading and absorption efficiency at 1 atm and 50 °C in MSR-2.

reported in literature [48,49].

3.4. Regeneration efficiency of the absorbent

Absorbent regeneration measures the cyclic capacity of an absorbent and it has a significant importance in evaluating the energy requirement of CO_2 absorption processes. This important characteristic was overlooked in most of CO_2 absorption studies executed in microreactors, as indicated by Table 7. Regeneration was performed by heating the rich solution in an oil bath at 120 °C for one hour, and the vapor was recovered by using a condenser. CO_2 loading in fresh and regenerated absorbents were used to determine the regeneration efficiency [50], as given by Eq. (24):

$$Rgeneration\ efficiency(\varphi) = \frac{CO_2\ loading\ in\ regenerated\ absorbent\ of\ i-cycle}{CO_2\ loading\ in\ fresh\ absorbent} \quad (24)$$

Fig. 9 compares the regeneration efficiency of three successive regenerated absorbents at various gas to liquid flow rate ratios. It should be noted that the second and third regenerated absorbents exhibited 12.6% and 20.3% lower regeneration efficiency than the first regenerated absorbent at the gas to liquid flow rate ratio of 400, but all three regenerated absorbents showed almost consistent regeneration efficiency at the gas to liquid flow rate ratios of 181.8 and 222.2. Thus, this gas to liquid flow rate ratio range (181.8–222.2) was possibly considered as an optimum range to attain the consistent regeneration efficiency. HMDA concentration was crucial to maintain the better regeneration efficiency in the successive regenerated absorbents. Therefore, ^{13}C NMR characterization was performed to investigate the concentration variation of MDEA and HMDA in the fresh and regenerated absorbents. It was performed through Bruker 500 by using D_2O as a solvent. Fig. 10 indicates the NMR spectra of the fresh and regenerated absorbents and details of chemical shifts and peak area are provided in the Supporting Information (Fig. S4). ^{13}C NMR spectra of all regenerated absorbents represented a new peak at 41.15 ppm in accordance with -CH_2 - NH that indicated the formation of carbamate [51]. The concentration ratio of MDEA and HMDA in the fresh absorbent was 5, and the same value was obtained from the peak area ratio of MDEA (C_4 and C_3) and HMDA (C_7 and C_4). This ratio was evaluated by a similar manner in the regenerated absorbents and it raised to 5.81, 6.12 and 6.35 in the first, second and third regenerated absorbents, respectively. This indicated that the HMDA concentration was gradually reduced after each regeneration cycle which triggered low regeneration efficiency in the subsequent regenerated absorbents.

3.5. CO_2 absorption flux and overall reaction rate constant

This section elaborates the influence of temperature and gas to liquid flow rate ratio on the absorption flux and overall reaction rate constant. Fig. 11 (a) shows the trends of absorption flux with time at three different gas to liquid flow rate ratios. Initially, the absorption flux sharply increased with the time, but it started to level off near the saturation condition. In fact, the viscosity of the absorbent increased upon the CO_2 absorption that restricted the diffusion and mass transport of CO_2 [51]. This saturation effect was greatly affected by the gas to liquid flow rate ratio. Fig. 11 (b) describes the enhancement of absorption flux by increasing the temperature. Liquid film was sharply saturated by rising the temperature. For instance, it was saturated only after ~150 s at 60 °C, but it had an ability to absorb more CO_2 even after 240 s at 30 °C and 40 °C. It should be noted that these values of CO_2 absorption flux were higher than those of the conventional absorbers [4,52].

Pseudo-first-order (PFO) reaction kinetics was utilized to determine the overall reaction rate constant, as mentioned in Section 2.4. Table 4 shows the overall reaction rate constant (k_{ov}), Hatta number (Ha) and enhancement factor (E) determined at three different gas to liquid flow

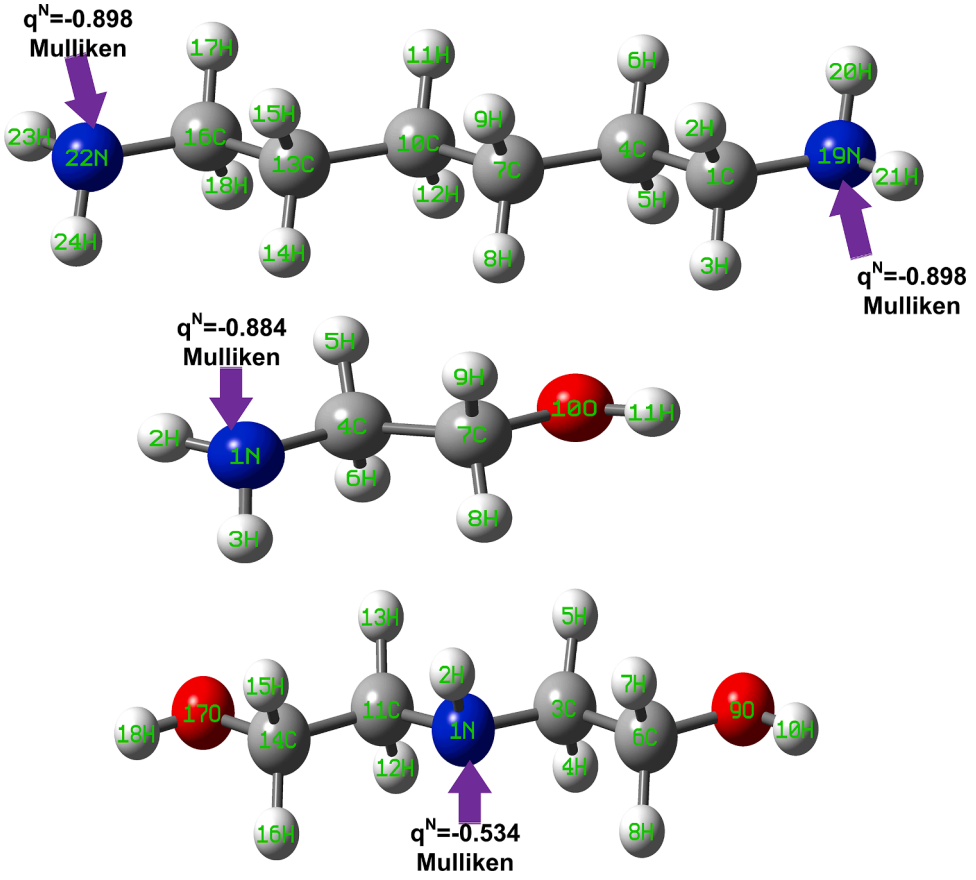

Fig. 8. Optimized molecular structures of various amines obtained through B3LYP density functional theory method in Gaussian 09.

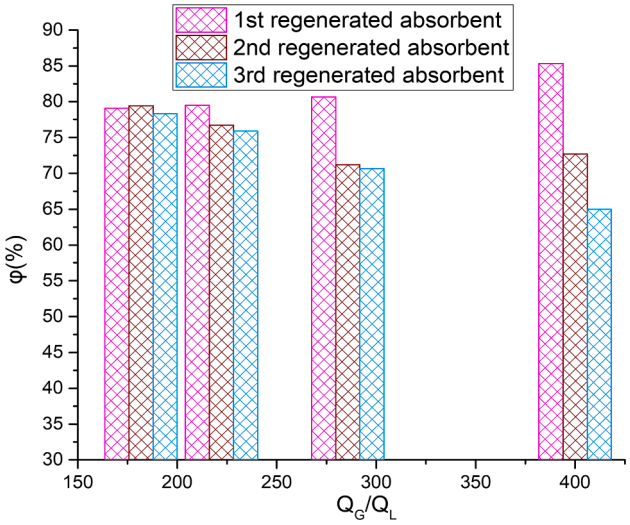

Fig. 9. Regeneration efficiencies of mixed amine absorbent (25 wt.% MDEA and 5 wt.% HMDA) in three subsequent regenerated cycles at 1 atm and 60 °C in MSR-2.

rate ratios. Each value of *Ha* was greater than 3 that fulfilled the pseudo-first-order reaction assumption. Furthermore, the enhancement factors of this mixed amine absorbent were comparable to those obtained for the conventional amines at low gas to liquid flow rate ratios [23,29]. Fig. 12 indicates the rising trends of the overall reaction rate constants with the temperature at three different gas to liquid flow rate ratios. It is worth mentioning that the overall reaction rate constants obtained from MSR-2 were 2–3 times higher than those of the reaction calorimeter [36].

The overall reaction rate constant implicates the additive contribution of MDEA and HMDA in the CO_2 absorption. Secondly, HMDA was used as a promotor and mainly involved in this CO_2 absorption as confirmed through ^{13}C NMR investigations in the previous section. Thus, $k_{2,HMDA}$ was accounted for the major contribution in k_{ov}. The kinetic expression for $k_{2,MDEA}$ was taken from the literature [53], as indicated by Eq.(26), while the remaining rate constants, including $k_{2,HMDA}$, $k_{2,HMDA}k_{H2O}/k_{-1}$, $k_{2,HMDA}k_{MDEA}/k_{-1}$ and $k_{2,HMDA}k_{HMDA}/k_{-1}$ exhibited insignificant contribution in k_{ov} and were regressed in the form of Arrhenius expressions through Eq. (17). The following objective function was minimized by using nonlinear least-square optimization through the Levenberg-Marquardt method.

$$OF = \frac{1}{N}\sum_{i=1}^{N}\left|\frac{k_{ov}^{exp} - k_{ov}^{mod}}{k_{ov}^{exp}}\right| \tag{25}$$

$$k_{2,MDEA} = 4.01 \times 10^{8} exp\left(\frac{-5400}{T}\right) \tag{26}$$

The regression of the kinetic data obtained at the flow rate ratios of 133.34, 177.78 and 222.23 was separately performed. Kinetic expression of $k_{2,HMDA}$ obtained at these gas to liquid flow rate ratios are given below:

$$k_{2,HMDA} = 3.26 \times 10^{4} exp\left(\frac{-260}{T}\right)\frac{Q_G}{Q_L} = 133.3 \tag{27}$$

$$k_{2,HMDA} = 4.25 \times 10^{4} exp\left(\frac{-195}{T}\right)\frac{Q_G}{Q_L} = 177.8 \tag{28}$$

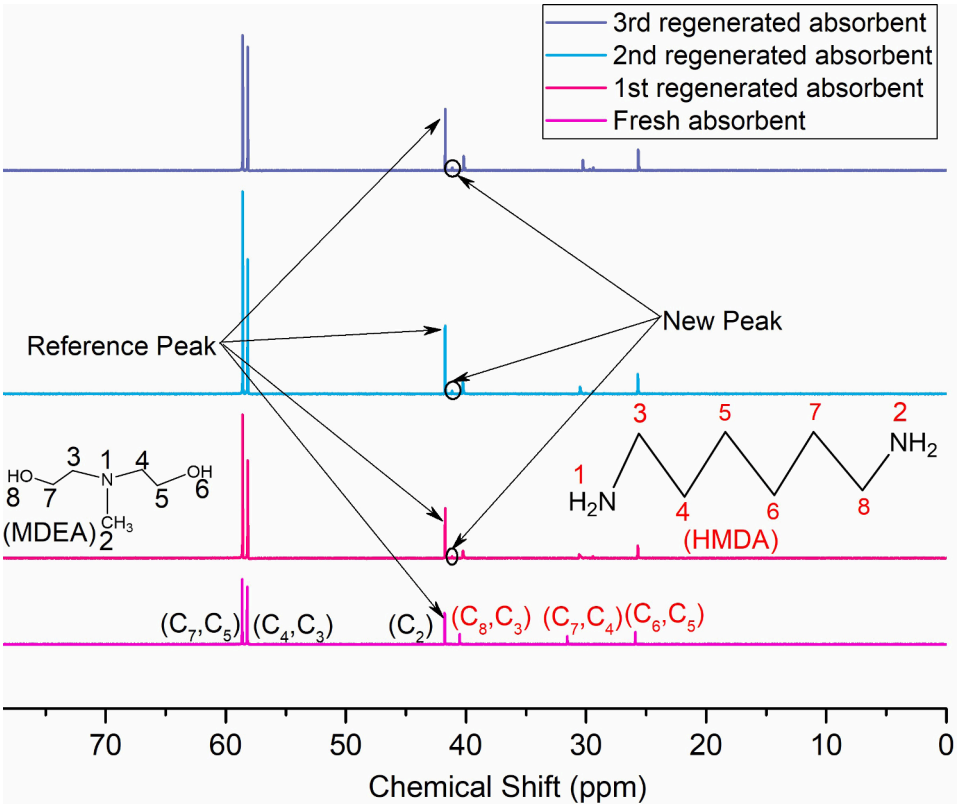

Fig.10. ^{13}C NMR Spectra of fresh and three regenerated absorbents.

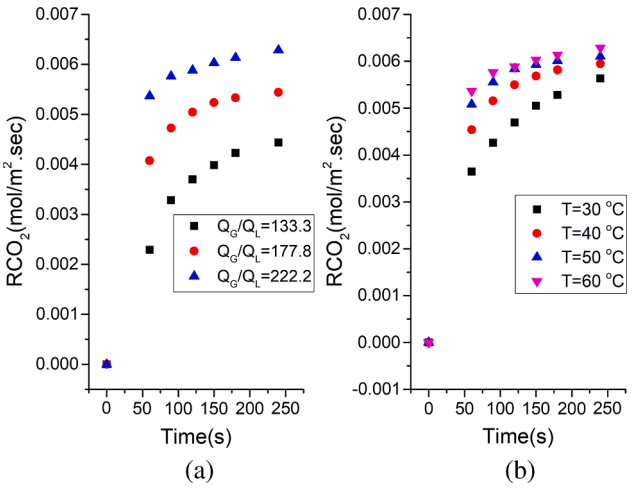

Fig. 11. Absorption flux (a) measured by varying flow rate ratio at 60 °C and 1 atm (b) measured by varying temperature at 1 atm and flow rate ratio of 222.2 in MSR-2.

$$k_{2,HMDA} = 5.92 \times 10^{4} exp\left(\frac{-148.5}{T}\right)\frac{Q_G}{Q_L} = 222.2 \quad (29)$$

The remaining rate constants, including $k_{2,HMDA}k_{H2O}/k_{-1}$, $k_{2,HMDA}k_{MDEA}/k_{-1}$ and $k_{2,HMDA}k_{HMDA}/k_{-1}$ were related to the deprotonation and reverse carbamate formation reactions of Scheme 2. These reaction rate constants could be expressed by Arrhenius equations and showed similar expressions at all three gas to liquid flow rate ratios, which are presented as follows:

$$\frac{k_{2,HMDA}k_{H_2O}}{k_{-1}} = 7.66 \times 10^{12} exp\left(\frac{-10500}{T}\right)\frac{Q_G}{Q_L} = 133.3, 177.8, 222.2 \quad (30)$$

Table 4
Kinetic parameters for CO_2 absorption using the aqueous mixed mine (25 wt.% MDEA and 5 wt.% HMDA) in MSR-2.

Flow rate ratio Q_G/Q_L	Temperature (K)	Overall reaction rate constant k_{ov} (s^{-1})	Enhancement factor E	Hatta Number Ha
133.3	303	3461.10	27.37	27.36
	313	4744.42	32.65	32.63
	323	5910.23	37.53	37.51
	333	6273.00	38.88	38.86
177.8	303	4887.25	29.61	29.60
	313	7129.61	36.57	36.55
	323	8749.72	41.65	41.64
	333	9866.27	44.00	43.99
222.2	303	6860.92	32.72	32.70
	313	9619.07	39.11	39.10
	323	11181.03	42.33	42.32
	333	11936.03	43.77	43.76

$$\frac{k_{2,HMDA}k_{MDEA}}{k_{-1}} = 2.14 \times 10^{18} exp\left(\frac{-11248}{T}\right)\frac{Q_G}{Q_L} = 133.3, 177.8, 222.2 \quad (31)$$

$$\frac{k_{2,HMDA}k_{HMDA}}{k_{-1}} = 4.50 \times 10^{19} exp\left(\frac{-10500}{T}\right)\frac{Q_G}{Q_L} = 133.3, 177.8, 222.2 \quad (32)$$

Fig. 13 presents the experimental and predicted k_{ov} obtained at the involved gas to liquid flow rate ratios, and the mean absolute percentage deviation (MAPD) between these values was estimated to be 7.29%, which is comparable to other studies [36]. Table 5 summarizes the second-order rate constants of various amines. It can be clearly visualized that the second-order rate constant of HMDA was much higher, and its potential energy barrier was considerably lower than the conventional amines. Consequently, the CO_2 absorption rate was significantly improved in MSR-2 by the addition of a small amount of HMDA.

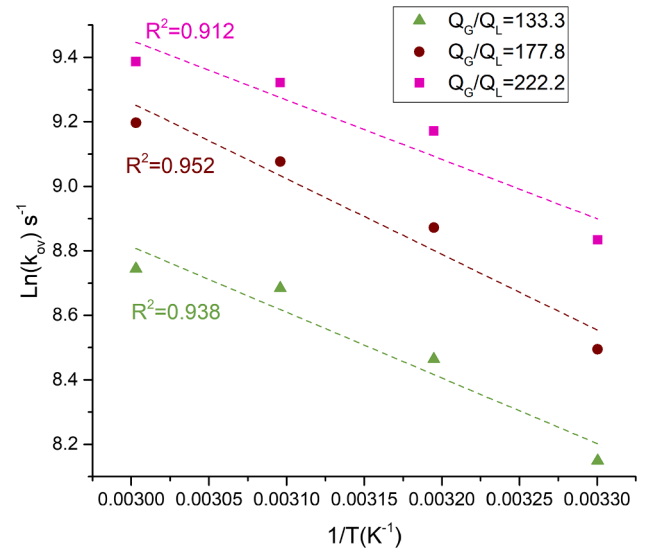

Fig. 12. Arrhenius plot of kinetic data obtained at three different flow rate ratios in MSR-2.

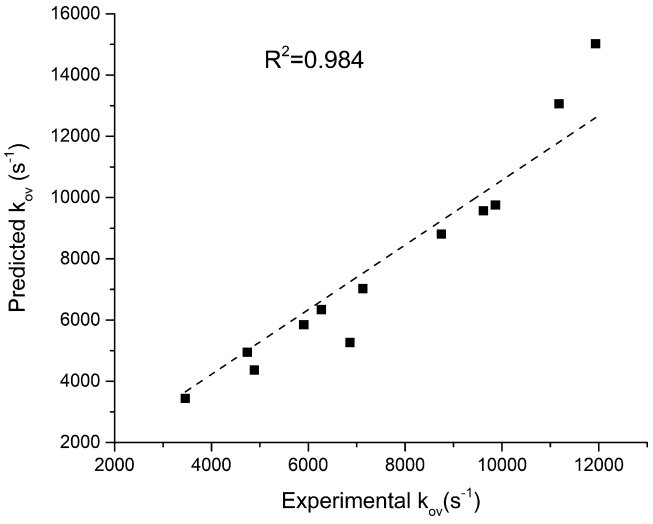

Fig. 13. Experimental and predicted overall rate constants.

3.6. Optimization of overall rate constants and mass transfer coefficients

Increase of the gas to liquid flow rate ratio triggered a tradeoff between the overall reaction rate constant and the overall volumetric mass transfer coefficient. Multi-objective optimization based on genetic algorithm was used to determine the optimum values of these parameters [54,55]. Gas to liquid flow rate ratio (x_1) and temperature (x_2) were taken as design variables, and objective functions of k_{ov} ($f_1(x_1,x_2)$) and k_La ($f_2(x_1,x_2)$) were developed in terms of these variables by using *curvefit* tool. Adjusted R^2 showed a value of 0.99 for both functions, as indicated in Fig. 14.

$$f_1(x_1,x_2) = -345200 - 174.28x_1 + 2146x_2 - 0.08113x_1^2 + 0.8084x_1x_2 - 3.375x_2^2 \quad (33)$$

$$f_2(x_1,x_2) = -407.8 + 0.3309x_1 + 2.317x_2 - 0.0004074x_1^2 - 0.0006773x_1x_2 - 0.003242x_2^2 \quad (34)$$

Main objective of this optimization is to maximize both objective functions and its problem formulation can be described through the following equation:

$$\begin{gathered} max(f_1(x_1,x_2),f_2(x_1,x_2)) \\ subjected\ to \\ h_k(x_1,x_2) = 0\ \forall\ k\ = 1,2...p \\ g_j(x_1,x_2) \leqslant 0\ \forall\ j = 1,2,...n \end{gathered} \quad (35)$$

where $h_k(x_1.x_2)$ and $g_j(x_1,x_2)$ are the equality and inequality constraint functions, respectively. The *gamultiobj* solver was used to perform this optimization, and the parameter setting of this solver is provided in the Supporting Information (Table S2). Fig. 15 indicates the pareto optimal front of both objective functions. The optimum ranges of the overall reaction rate constant and the mass transfer coefficient were varied from 9624.6 to 12248.1 s^{-1} and 7.56 to 10.02 s^{-1}, respectively. Moreover, these optimum values were achieved at the gas to liquid flow rate ratio ranging from 180 to 222.1, which was almost identical to the optimum gas to liquid flow rate ratio of the regeneration efficiency (181.8–222.2). However, the optimum temperature was maintained at 60 °C, as a high temperature was favorable for the maximization of both objective functions.

Validation of these optimization results was performed through the experimentation. Five random values of k_{ov} and k_La were selected from the pareto optimal front and re-evaluated them through experiments, as indicated in Table 6. There was a good agreement between the optimum values of k_{ov} and k_La obtained through experiment and optimization algorithm with the MAPD of 4.05% and 2.45%, respectively.

3.7. Comparison among various microreactors for CO_2 absorption processes

Finally, a comprehensive comparison between the MSR-2 and other microreactors is presented to analyze their scale-up potential. This analysis is benchmarked using various key performance indicators for CO_2 absorption, including overall volumetric mass transfer coefficient, absorption efficiency, CO_2 loading and regeneration efficiency of the absorbent and operating range, which is presented in terms of the gas to liquid flow rate ratio, as indicated by Table 7. MSR-2 outperformed the other microreactors at high gas to liquid flow rate ratio because of its excellent values of key performance parameters for CO_2 absorption. For instance, the CO_2 uptake ability of this amine reached 0.32 mol of CO_2/ mol of MDEA with CO_2 partial pressure of 10 kPa, which was much higher than conventional amines. In one study, the CO_2 loading reached to 0.30 mol of CO_2/ mol of DEA [24], but this investigation was performed at the CO_2 partial pressure of 400 kPa. Moreover, Sang et al. [26] also applied aqueous MDEA for CO_2 absorption in micropacked bed reactors with metal foams, but the absence of promotor in MDEA resulted in inferior mass transfer performance compared to our current MSR-2.

Secondly, the absorbent regeneration efficiency was not determined in most of CO_2 absorption studies, but this mixed amine absorbent (25 wt.% MDEA and 5 wt.% HMDA) exhibited high and consistent regeneration efficiency in the three successive regenerated cycles. Although the overall volumetric mass transfer coefficients obtained in MSR-2 were lower than other microreactors reported in literature, but these k_La values were achieved at much higher gas to liquid flow rate ratios. Moreover, the absorption efficiencies in MSR-2 were almost consistent with the other microreactors even they were obtained at much higher gas to liquid flow rate ratios. The excellent process intensification of this

Table 5
Kinetic data of CO_2 absorption processes in various reactors.

Amine absorbent	Conc.	Reactors type	Temp. (K)	Kinetic expression	Activation energy (kJ/mol)	Ref.
MEA	30 wt.%	Microchannel	298–318	$k_{2,MEA} = 1.09 \times 10^9 exp\left(\frac{-2671.4}{T}\right)$	22.21	[31]
AMP	1 M	Microcontactor	298–318	$k_{2,AMP} = 2.95 \times 10^7 exp\left(\frac{-3152}{T}\right)$	26.21	[42]
HMDA	5–30 wt.%	Reaction calorimeter	303–333	$k_{2,HMDA} = 2.4 \times 10^9 exp\left(\frac{-3321}{T}\right)$	27.61	[48]
MDEA + HMDA	15–25 wt.% (MDEA) 5–15 wt.% (HMDA)	Reaction calorimeter	303–333	$k_{2,HMDA} = 8.42 \times 10^4 exp\left(\frac{-478}{T}\right)$	3.97	[36]
MDEA + Ionic liquid (IL)	Mole ratio of MDEA and IL (8:2)	Stirred-cell absorber	303–333	$k_2 = 1.398 \times 10^{15} exp\left(\frac{-9176.6}{T}\right)$	76.29	[4]
MDEA + HMDA	25 wt.% (MDEA) 5 wt.% (HMDA)	MSR-2	303–333	$k_{2,HMDA} = 5.92 \times 10^4 exp\left(\frac{-148.5}{T}\right)$	1.23	This work

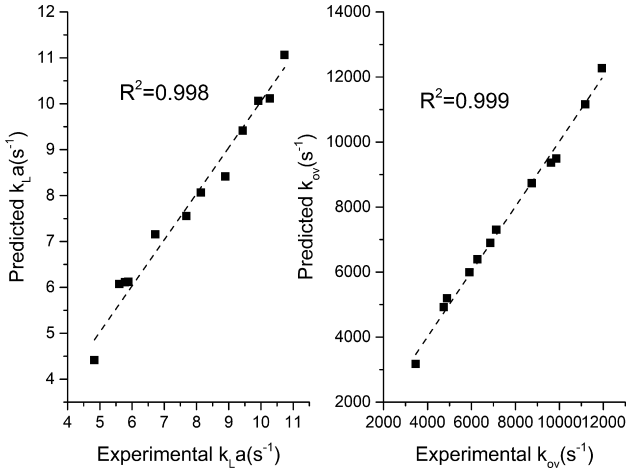

Fig. 14. Predicted and experimental data of overall volumetric mass transfer coefficients and overall rate constants.

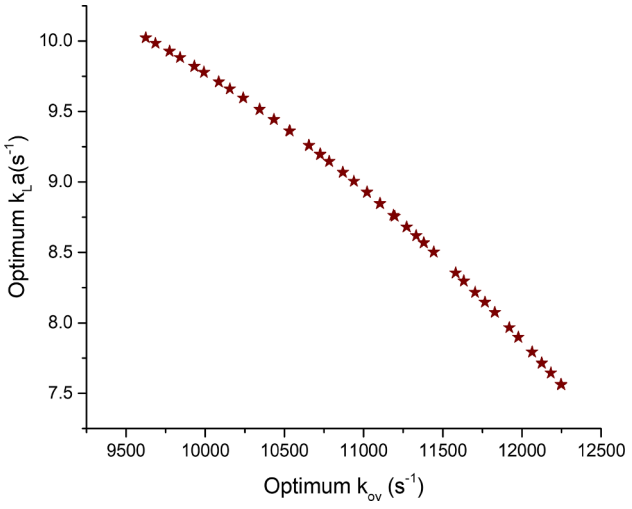

Fig. 15. Pareto optimal front of overall rate constant and overall volumetric mass transfer coefficient.

microstructured reactor shows its great scale-up potential for the removal of CO_2 from industrial flue gases through the numbering-up strategy.

4. Conclusion

Mass transfer and kinetic characteristics of CO_2 absorption in microstructured reactors with metal foams as packing materials were investigated by using an aqueous mixed amine absorbent (25 wt.% MDEA + 5 wt.% HMDA). These investigations were performed at high gas to liquid flow rate ratios, ranging from 88.9 to 666.7. Mass transfer performance was drastically improved by rising the temperature and the HMDA concentration. The overall volumetric mass transfer coefficient and the absorption efficiency respectively reached 13.5 s^{-1} and 97% at the gas to liquid flow rate ratios of 153.8 and 88.9, which are higher than those reported for other microreactors used for CO_2 absorption. This mixed amine absorbent exhibited excellent CO_2 loading and regeneration efficiency in the three successive regenerated cycles. In particular, the CO_2 loading of this amine absorbent was seventeen times higher than that of aqueous MDEA (30 wt.% MDEA) at the gas to liquid flow rate ratio of 400.

The kinetic characteristics were measured at three different gas to liquid flow ratios by varying the temperature from 303 to 333 K. The second-order rate constant of HMDA was higher, and its potential energy barrier was lower than conventional amines. Overall reaction rate constants obtained in MSR-2 were 2–3 times higher than those of the reaction calorimeter. The tradeoff between overall reaction rate constant and mass transfer coefficient was resolved through the multi-objective optimization based on the genetic algorithm and the validation of these results was performed through the experimentation. Overall, the microstructured reactors with metal foams as packing materials in combination with remarkable CO_2 uptake ability of this specific mixed amine absorbent showed great improvement in the mass transfer and kinetic characteristics of CO_2 absorption at high gas to liquid flow rate ratios.

Table 6
Experimental validation of optimization data.

Optimum flow ratio	Optimum temperature (K)	Optimum k_{ov} (s^{-1})		Optimum k_La (s^{-1})	
		Genetic algorithm	Experiment	Genetic algorithm	Experiment
182.29	333	9774.11	9175.61	9.93	9.90
188.15	333	10154.56	9821.24	9.66	9.87
195.99	333	10654.62	10198.79	9.26	9.39
200.53	333	10938.94	10730.94	9.00	9.20
210.96	333	11581.03	11140.37	8.35	8.92

Table 7
Mass transfer performance comparison of MSR-2 with other microreactors.

Gas to liquid flow ratio	Microreactor details	Overall mass transfer coefficient k_La (s^{-1})	Absorption efficiency η (%)	CO_2 Loading α (mol of CO_2/mol of amine) @10 kPa of CO_2	Regeneration efficiency ϕ (%)	Reference
1.5–75	Numbered-up (ID = 0.456 mm)	5.0–17.0	40–99	0.005–0.13	–	[30]
0.015–260	Numbered-up	1.59–90	45–97	0.28–0.30	–	[24]
4.5–22.75	Single microchannel (ID = 0.254, 0.508 , 0.762 mm)	35–400	40–99	–	–	[23]
2.5–60	Micropacked bed reactor with Ni metal foams	0.09–0.38	–	–	–	[26]
88.9–666.7	Microstructured reactor (MSR-2)	1.25–13.5	23–97	0.10–0.32	65–85	This study

CRediT authorship contribution statement

Mohsin Pasha: Data curation, Formal analysis, Investigation, Methodology, Project administration, Software, Validation, Writing - original draft, Writing - review & editing. **Guangxiao Li:** Investigation, Methodology. **Minjing Shang:** Supervision. **Saier Liu:** Investigation, Methodology. **Yuanhai Su:** Funding acquisition, Conceptualization, Supervision, Writing - original draft, Writing - review & editing.

Declaration of Competing Interest

The authors declare that they have no known competing financial interests or personal relationships that could have appeared to influence the work reported in this paper.

Acknowledgement

We acknowledge gratefully the financial supports for the project from the National Natural Science Foundation of China (No. 92034303), Science and Technology Commission of Shanghai Municipality (No: 18520743500) and the Shanghai Jiao Tong University Scientific and Technological Innovation Funds (No: 2019QYB06).

Appendix A. Supplementary material

Supplementary data to this article can be found online at https://doi.org/10.1016/j.seppur.2021.118987.

References

[1] X. Lim, How to make the most of carbon dioxide, Nat. News 526 (2015) 628.
[2] N.K. Vishwakarma, A.K. Singh, Y.-H. Hwang, D.-H. Ko, J.-O. Kim, A.G. Babu, D.-P. Kim, Integrated CO_2 capture-fixation chemistry via interfacial ionic liquid catalyst in laminar gas/liquid flow, Nat. Commun. 8 (2017) 14676.
[3] A. Uma Maheswari, K. Palanivelu, Carbon dioxide capture and utilization by alkanolamines in deep eutectic solvent medium, Ind. Eng. Chem. Res. 54 (2015) 11383–11392.
[4] C. Sun, S. Wen, J. Zhao, C. Zhao, W. Li, S. Li, D. Zhang, Mechanism and kinetics study of CO2 absorption into blends of N-methyldiethanolamine and 1-hydroxyethyl-3-methylimidazolium glycine aqueous solution, Energy Fuels 31 (2017) 12425–12433.
[5] S. Roussanaly, A. Aasen, R. Anantharaman, B. Danielsen, J. Jakobsen, L. Heme-De-Lacotte, G. Neji, A. Sødal, P. Wahl, T. Vrana, Offshore power generation with carbon capture and storage to decarbonise mainland electricity and offshore oil and gas installations: A techno-economic analysis, Appl. Energy 233 (2019) 478–494.
[6] W.H. Tay, K.K. Lau, L.S. Lai, A.M. Shariff, T. Wang, Current development and challenges in the intensified absorption technology for natural gas purification at offshore condition, J. Nat. Gas Sci. Eng. 71 (2019), 102977.
[7] B. Dutcher, M. Fan, A.G. Russell, Amine-based CO_2 capture technology development from the beginning of 2013—A review, ACS Appl. Mater. Interfaces 7 (2015) 2137–2148.
[8] R.S. Haszeldine, Carbon capture and storage: how green can black be? Science 325 (2009) 1647.
[9] D.M. D'Alessandro, B. Smit, J.R. Long, Carbon dioxide capture: prospects for new materials, Angew. Chem. Int. Ed. 49 (2010) 6058–6082.
[10] K.S. Elvira, X.C.I. Solvas, R.C.R. Wootton, A.J. deMello, The past, present and potential for microfluidic reactor technology in chemical synthesis, Nat. Chem. 5 (2013) 905–915.
[11] R.L. Hartman, J.P. McMullen, K.F. Jensen, Deciding whether to go with the flow: evaluating the merits of flow reactors for synthesis, Angew. Chem. Int. Ed. 50 (2011) 7502–7519.
[12] S. Lladó Maldonado, D. Rasch, A. Kasjanow, D. Bouwes, U. Krühne, R. Krull, Multiphase microreactors with intensification of oxygen mass transfer rate and mixing performance for bioprocess development, Biochem. Eng. J. 139 (2018) 57–67.
[13] S. Asano, S. Yatabe, T. Maki, K. Mae, Numerical and experimental quantification of the performance of microreactors for scaling-up fast chemical reactions, Org. Process Res. Dev. 23 (2019) 807–817.
[14] Y. Song, M. Shang, G. Li, Z.-H. Luo, Y. Su, Influence of mixing performance on polymerization of acrylamide in capillary microreactors, AIChE J. 64 (2018) 1828–1840.
[15] E.Y. Kenig, Y. Su, A. Lautenschleger, P. Chasanis, M. Grünewald, Micro-separation of fluid systems: A state-of-the-art review, Sep. Purif. Technol. 120 (2013) 245–264.
[16] A. Pohar, I. Plazl, Process intensification through microreactor application, Chem. Biochem. Eng. Q. 23 (2009) 537–544.
[17] G. Chen, J. Yue, Q. Yuan, Gas-liquid microreaction technology: recent developments and future challenges, Chin. J. Chem. Eng. 16 (2008) 663–669.
[18] H. Shi, K. Nie, B. Dong, M. Long, H. Xu, Z. Liu, Recent progress of microfluidic reactors for biomedical applications, Chem. Eng. J. 361 (2019) 635–650.
[19] T. Tian, J. Li, Y. Song, L. Zhou, Z. Zhu, C.J. Yang, Distance-based microfluidic quantitative detection methods for point-of-care testing, Lab Chip 16 (2016) 1139–1151.
[20] J. Shen, Y. Zhao, G. Chen, Q. Yuan, Investigation of nitration processes of iso-octanol with mixed acid in a microreactor, Chin. J. Chem. Eng. 17 (2009) 412–418.
[21] H. Ge, G. Chen, Q. Yuan, H. Li, Gas phase partial oxidation of toluene over modified V2O5/TiO2 catalysts in a microreactor, Chem. Eng. J. 127 (2007) 39–46.
[22] Y. Song, J. Song, M. Shang, W. Xu, S. Liu, B. Wang, Q. Lu, Y. Su, Hydrodynamics and mass transfer performance during the chemical oxidative polymerization of aniline in microreactors, Chem. Eng. J. 353 (2018) 769–780.
[23] H. Ganapathy, A. Shooshtari, S. Dessiatoun, M. Ohadi, M. Alshehhi, Hydrodynamics and mass transfer performance of a microreactor for enhanced gas separation processes, Chem. Eng. J. 266 (2015) 258–270.
[24] C. Yao, K. Zhu, Y. Liu, H. Liu, F. Jiao, G. Chen, Intensified CO_2 absorption in a microchannel reactor under elevated pressures, Chem. Eng. J. 319 (2017) 179–190.
[25] M.-Y. Pan, Z. Qian, L. Shao, M. Arowo, J.-F. Chen, J.-X. Wang, Absorption of carbon dioxide into N-methyldiethanolamine in a high-throughput microchannel reactor, Sep. Purif. Technol. 125 (2014) 52–58.

[26] L. Sang, J. Tu, H. Cheng, G. Luo, J. Zhang, Hydrodynamics and mass transfer of gas–liquid flow in micropacked bed reactors with metal foam packing, AIChE J. 66 (2020), e16803.
[27] S. Voltolina, P. Marín, F.V. Díez, S. Ordóñez, Open-cell foams as beds in multiphase reactors: Residence time distribution and mass transfer, Chem. Eng. J. 316 (2017) 323–331.
[28] I. Mohammed, T. Bauer, M. Schubert, R. Lange, Hydrodynamic multiplicity in a tubular reactor with solid foam packings, Chem. Eng. J. 231 (2013) 334–344.
[29] H. Ganapathy, A. Shooshtari, S. Dessiatoun, M. Alshehhi, M. Ohadi, Fluid flow and mass transfer characteristics of enhanced CO_2 capture in a minichannel reactor, Appl. Energy 119 (2014) 43–56.
[30] H. Ganapathy, S. Steinmayer, A. Shooshtari, S. Dessiatoun, M.M. Ohadi, M. Alshehhi, Process intensification characteristics of a microreactor absorber for enhanced CO_2 capture, Appl. Energy 162 (2016) 416–427.
[31] C. Ye, M. Dang, C. Yao, G. Chen, Q. Yuan, Process analysis on CO_2 absorption by monoethanolamine solutions in microchannel reactors, Chem. Eng. J. 225 (2013) 120–127.
[32] B. Aghel, E. Heidaryan, S. Sahraie, S. Mir, Application of the microchannel reactor to carbon dioxide absorption, J. Cleaner Prod. 231 (2019) 723–732.
[33] B. Aghel, S. Sahraie, E. Heidaryan, K. Varmira, Experimental study of carbon dioxide absorption by mixed aqueous solutions of methyl diethanolamine (MDEA) and piperazine (PZ) in a microreactor, Process Saf. Environ. Prot. 131 (2019) 152–159.
[34] H. Niu, L. Pan, H. Su, S. Wang, Effects of design and operating parameters on CO_2 absorption in microchannel contactors, Ind. Eng. Chem. Res. 48 (2009) 8629–8634.
[35] G. Lin, S. Jiang, C. Zhu, T. Fu, Y. Ma, Mass-transfer characteristics of CO_2 absorption into aqueous solutions of N-methyldiethanolamine+ diethanolamine in a T-junction microchannel, ACS Sustain. Chem. Eng. 7 (2019) 4368–4375.
[36] B.K. Mondal, S.S. Bandyopadhyay, A.N. Samanta, Kinetics of CO_2 absorption in aqueous hexamethylenediamine blended N-methyldiethanolamine, Ind. Eng. Chem. Res. 56 (2017) 14902–14913.
[37] A. Samanta, S.S. Bandyopadhyay, Absorption of carbon dioxide into piperazine activated aqueous N-methyldiethanolamine, Chem. Eng. J. 171 (2011) 734–741.
[38] J. Zhang, A.R. Teixeira, K.F. Jensen, Automated measurements of gas-liquid mass transfer in micropacked bed reactors, AIChE J. 64 (2018) 564–570.
[39] J.-N. Tourvieille, R. Philippe, C. de Bellefon, Milli-channel with metal foams under an applied gas–liquid periodic flow: flow patterns, residence time distribution and pulsing properties, Chem. Eng. Sci. 126 (2015) 406–426.
[40] P. Singh, W.P.M. van Swaaij, D.W.F. Brilman, Kinetics study of carbon dioxide absorption in aqueous solutions of 1,6-hexamethyldiamine (HMDA) and 1,6-hexamethyldiamine, N, N′ di-methyl (HMDA, N, N′), Chem. Eng. Sci. 66 (2011) 4521–4532.
[41] G.F. Versteeg, W.P.M. van Swaaij, On the kinetics between CO_2 and alkanolamines both in aqueous and non-aqueous solutions—I. Primary and secondary amines, Chem. Eng. Sci. 43 (1988) 573–585.
[42] C. Zheng, B. Zhao, K. Wang, G. Luo, Determination of kinetics of CO_2 absorption in solutions of 2-amino-2-methyl-1-propanol using a microfluidic technique, AIChE J. 61 (2015) 4358–4366.
[43] M. Roudet, K. Loubiere, C. Gourdon, M. Cabassud, Hydrodynamic and mass transfer in inertial gas–liquid flow regimes through straight and meandering millimetric square channels, Chem. Eng. Sci. 66 (2011) 2974–2990.
[44] Y. Chen, Y. Zhao, M. Han, C. Ye, M. Dang, G. Chen, Safe, efficient and selective synthesis of dinitro herbicides via a multifunctional continuous-flow microreactor: one-step dinitration with nitric acid as agent, Green Chem. 15 (2013) 91–94.
[45] J. Yue, G. Chen, Q. Yuan, L. Luo, Y. Gonthier, Hydrodynamics and mass transfer characteristics in gas–liquid flow through a rectangular microchannel, Chem. Eng. Sci. 62 (2007) 2096–2108.
[46] J.W. Coleman, S. Garimella, Characterization of two-phase flow patterns in small diameter round and rectangular tubes, Int. J. Heat Mass Transf. 42 (1999) 2869–2881.
[47] D. Luo, S.M. Ghiaasiaan, Liquid-side interphase mass transfer in cocurrent vertical two-phase channel flows, Int. J. Heat Mass Transf. 40 (1997) 641–655.
[48] B.K. Mondal, S.S. Bandyopadhyay, A.N. Samanta, Kinetics of CO_2 absorption in aqueous hexamethylenediamine, Int. J. Greenhouse Gas Control 56 (2017) 116–125.
[49] P. Singh, Amine based solvent for CO2 absorption : From molecular structure to process, Doctoral Thesis, in, University of Twente, Netherlands 2011.
[50] B. Lv, Y. Shi, C. Sun, N. Liu, W. Li, S. Li, CO_2 capture by a highly-efficient aqueous blend of monoethanolamine and a hydrophilic amino acid ionic liquid [C_2OHmim][Gly], Chem. Eng. J. 270 (2015) 372–377.
[51] T.J. Trivedi, J.H. Lee, H.J. Lee, Y.K. Jeong, J.W. Choi, Deep eutectic solvents as attractive media for CO_2 capture, Green Chem. 18 (2016) 2834–2842.
[52] A. Ahmady, M.A. Hashim, M.K. Aroua, Kinetics of Carbon Dioxide absorption into aqueous MDEA+[bmim][BF4] solutions from 303 to 333K, Chem. Eng. J. 200–202 (2012) 317–328.
[53] J.-J. Ko, M.-H. Li, Kinetics of absorption of carbon dioxide into solutions of N-methyldiethanolamine+water, Chem. Eng. Sci. 55 (2000) 4139–4147.
[54] M. Mansour, K. Zähringer, K.D.P. Nigam, D. Thévenin, G. Janiga, Multi-objective optimization of liquid-liquid mixing in helical pipes using Genetic Algorithms coupled with Computational Fluid Dynamics, Chem. Eng. J. 391 (2020), 123570.
[55] J. Na, K.S. Kshetrimayum, U. Lee, C. Han, Multi-objective optimization of microchannel reactor for Fischer-Tropsch synthesis using computational fluid dynamics and genetic algorithm, Chem. Eng. J. 313 (2017) 1521–1534.